LA-UR-88-4213

Los Alamos National Laboratory is operated by the University of California for the United States Department of Energy under contract W-7405-ENG-36

TITLE ANALYSIS OF THE STRAIN-RATE SENSITIVITY AT HIGH STRAIN RATES IN FCC AND BCC METALS

LA-UR--88-4213

DE89 005471

AUTHOR(S) Paul S. Follansbee

SUBMITTED TO Fourth Oxford Conference on: The Mechanical Properties of Materials at High Rates of Strain
March 19-22, 1989
University of Oxford
Oxford, England

DISCLAIMER

LOS ALAMOS Los Alamos National Laboratory
Los Alamos, New Mexico 87545

Analysis of the Strain-Rate Sensitivity at High Strain Rates in FCC and BCC Metals

Paul S. Follansbee

Los Alamos National Laboratory, Los Alamos, NM, 87545, USA

ABSTRACT: The development of a constitutive model based on the use of internal state variables and phenomenological models describing glide kinetics is reviewed. Application of the model to the deformation of fcc metals and alloys is illustrated, with an emphasis on the behavior at high strain rates. Preliminary results in pure iron and 4340 steel are also presented. Deformation twinning is observed in iron samples deformed in the Hopkinson pressure bar. The influence of twinning on the proposed constitutive formalism is discussed.

1. INTRODUCTION

At the previous Oxford International Conference, Follansbee, Kocks, and Regazzoni (1984) analyzed the requirements for a transition in deformation mechanism from thermal activation control to dislocation drag control with increasing strain rate . Measurements in OFE copper were presented along with the predictions of an analysis based on

$$\dot{\varepsilon} = \frac{\rho_m b \lambda}{t_w + t_r}, \qquad (1)$$

where ρ_m is the mobile dislocation density, b is the Burgers vector, λ is the mean spacing between obstacles, t_w is time spent waiting for thermal activation energy to assist the overcoming of a characteristic obstacle, and t_r is the time spent running (under phonon drag control) between obstacles. The waiting time was represented with a Boltzmann equation of the form

$$t_w = \nu_0^{-1} \exp\left[\frac{\Delta G(\sigma/\hat{\sigma})}{kT}\right], \qquad (2)$$

where ν_0 is the jump frequency, k is the Boltzmann constant, T is the temperature, and σ is the applied stress. The mechanical threshold stress $\hat{\sigma}$ is the applied stress required at absolute zero where there can be no thermal contribution, and is a measure of the state of the material. Equation (1) is only strictly valid as a description of the strain-rate dependence at a constant state. One way to satisfy this requirement would be to use measurements of the yield stress. In the high strain rate regime, however, accurate measurements of the yield stress are difficult, whereas accurate measurements of the flow stress at, say $0.1 < \varepsilon < 0.2$, are possible to strain rates as high as 10^4 s^{-1}. Follansbee et al (1984) measured $\hat{\sigma}$ on samples deformed at $\dot{\varepsilon} = 5000$ s^{-1} to a strain of $\varepsilon = 15\%$, and, assuming that the mechanical threshold stress was not dependent on the strain rate (i.e., assuming that constant strain was equivalent to constant state), the strain rate variation predicted by Eq. (1) was compared with experimental results. The conclusion in this work was that the applied stresses remained below the mechanical threshold stress at

even the highest strain rates possible in a split Hopkinson pressure bar, and that Eq. (1) could not be made to fit the experimental results unless the mobile dislocation density was given a stress dependence.

In subsequent work, Follansbee (1985) and Follansbee, Kocks, and Regazzoni (1985) verified that the mechanical threshold stress measured on copper samples deformed to the same strain varied with the imposed strain rate, and that the strain-rate variation became stronger at high strain rates. This implied that in order to evaluate Eq. (1) at a constant state, the strain-rate dependence of structure evolution had to be separated from the strain-rate dependence at constant structure. Follansbee and Kocks (1988) did this for copper, and Fig. 1 shows the resulting variation with strain rate of the flow stress at constant strain compared to the variation of the flow stress at constant threshold stress. Note that in the latter the dramatically increased strain-rate dependence at high strain rates disappears.

The purpose of this paper is to briefly review the model that was applied to the deformation of copper and to review the status of its application to other fcc metals and to bcc metals. Particular attention will be given to the description of behavior at high strain rates.

2. THE MECHANICAL THRESHOLD STRESS MODEL.

This model has been described in detail by Kocks (1976), Follansbee and Kocks (1988), Follansbee (1988a, 1988b), and Follansbee and Gray (1989). The applied stress required for deformation at any state (the yield stress) is written as a combination of an athermal component, σ_a, and several thermally activated components as

$$(\sigma - \sigma_a)^n = \sum_i^k \left[s_i(\dot{\varepsilon}, T)\ \hat{\sigma}_i \right]^n , \qquad (3)$$

where $\hat{\sigma}_i$ gives the mechanical threshold stress that characterizes the interaction of dislocations with obstacle i, s_i specifies the kinetics of those interactions, k is the number of separate obstacle contributions, and n is a power that accounts for the interactions between different types of obstacles ($1<n<2$). The s-values are derived from Eq. (2) with the free energy described by an expression of the form

$$\Delta G = g_{0i}\, \mu b^3 \left[1 - \left(\frac{\sigma_i}{\hat{\sigma}_i} \right)^p \right]^q , \qquad (4)$$

where g_{0i} is the normalized total activation energy, μ is the temperature dependent shear modulus, and p and q are constants that characterize the shape of the obstacle profile ($0<p<1$, $1<q<2$). When $\dot{\varepsilon}_w = \dot{\varepsilon}_i$, s_i can be derived from Eqs. (1-4) to equal

$$s_i = \left\{ 1 - \left[\frac{kT}{g_{0i}\mu b^3} \ln \frac{\dot{\varepsilon}_0}{\dot{\varepsilon}} \right]^{1/q} \right\}^{1/p} , \qquad (5)$$

where $\dot{\varepsilon}_0$ is a combination of ρ_m, b, λ, and ν, and is considered to be a constant and g_{0i}, p_i, and q_i can vary with obstacle type.

Equations (3 and 5) describe the variation of the yield strength for a given state. Strain hardening leads to an evolution of the state, through an increasing dislocation density. Evolution is treated differentially according to

$$\frac{d\hat{\sigma}_i}{d\varepsilon} = \theta_0(i) \left[1 - f\left(\frac{\hat{\sigma}_i}{\hat{\sigma}_{is}} \right) \right] \qquad (6)$$

where σ_f is the mechanical threshold stress that characterizes dislocation/dislocation interactions, σ_{fs} is the temperature and strain-rate dependent saturation value of σ_f, and θ_o is the Stage II hardening rate. When the function F equals unity, Eq. (6) defines the Voce law; the previous work in copper showed that a more complicated function F had to be used to approximate the transition to State IV deformation that occurs at large strains.

The Stage II hardening rate had previously been considered to be a constant (of order $\mu/20$), but the work in copper led to the conclusion that when the strain rate was raised above $\approx 10^3$ s^{-1}, the Stage II hardening rate took on a mild strain-rate dependence that resulted in rapid hardening and higher flow stresses. It was proposed (Follansbee, 1988a) that the strain-rate dependence of θ_o could be a result of the high stresses required for deformation in the near yield regime where the dislocation density is low. One of the implications of this is that the high strain-rate dependence of the flow stress should not be found in samples prestrained at low strain rates then reloaded in the split Hopkinson pressure bar. Figure 2 shows measurements in copper of the flow stress at 10% strain on annealed material and on samples prestrained 16.3% at $\dot{\varepsilon}=10^{-3}$ s^{-1} followed by 5% at the high strain rate. The strain-rate sensitivity is indeed lower for the prestrained material than for annealed material. The solid lines in this figure show predictions from the model described by Follansbee and Kocks (1988). The agreement with experimental results is good for the samples with no prestrain, but the model underpredicts the stresses for the prestrained samples. The dashed line shows the predicted stress levels at a strain of 21.3% at the high strain rate indicated. Note that following a strain rate increase, the flow stress approaches the level for deformation solely at the higher strain rate more rapidly than is predicted. This discrepancy between the model and the experimental results was noted previously (see Fig. 12 in Follansbee and Kocks, 1988).

While the origin of the strain-rate dependence of θ_o remains open, a contribution of this previous work is the observation that the behavior at high strain rates is dominated by this term, rather than by $\sigma(\dot{\varepsilon},T)$ in Eq. (3) or $\sigma_{fs}(\dot{\varepsilon},T)$ in Eq. (5). The resulting constitutive description is well suited for extrapolation to regimes of strain rate, strain, and temperature that are not easily evaluated experimentally, which is a distinct advantage over other constitutive descriptions that have been proposed for the high strain rate deformation of copper.

3. APPLICATION TO OTHER FCC METALS

In copper, dislocation/dislocation interactions provide the only thermally activated contribution to the flow stress, in addition to the small grain boundary component, which is considered to be athermal. This simplifies the analysis in that k=1 and thus n=1 in Eq. (3). The same is true in pure nickel, and in fact Follansbee et al (1989) have shown that nickel behaves very much like copper. This is illustrated in Fig. 3 which shows the variation of the Stage II hardening rate versus strain rate for nickel along with the previous results for copper.

The study of fcc alloys introduces the complexity of k>1 in Eq. (3). In Ni-C alloys, for example, carbon goes to interstitial sites which yields a more rate dependent strengthening contribution than found in pure fcc metals. Measurements in Ni-510 ppm C and Ni-1900 ppm C have been analyzed by summing the interstitial contribution along with the strain dependent

dislocation contribution with k=1.5 (Follansbee et al, 1989). Alloying with carbon also is found to influence the rate of hardening through the $\sigma_{fs}(\dot{\epsilon},T)$ term in Eq. (6). Finally, carbon has sufficient mobility in the nickel lattice to promote dynamic strain aging at quasi-static strain rates and room temperature. The contribution of strain aging is not included in the formalism outlined in the previous section.

Austenitic stainless steels represent a class of alloys with numerous engineering applications. As in the Ni-C alloys, the addition of interstitial atoms (e.g., C, N, O) and substitutional atoms (e.g., Cr, Ni, Al) lead to strongly rate-dependent deformation. In our work, the threshold stress is estimated by measuring the strain rate and temperature dependence of the yield stress on identical samples (either annealed or prestrained along a prescribed strain rate and temperature path) and then extrapolating to T=0K according to Eqs. (3 and 5). With k=n=1 the extrapolation is straightforward, but with k>1 there are too many unknowns in these equations to allow a unique solution. The Ni-C study was designed to systematically study the application of these equations by starting with pure nickel and then adding small amounts of carbon. The situation in austenitic stainless steels is too complex to easily separate each strengthening contribution. However, we can begin by defining two classses: those that evolve with strain and those that are present in the annealed condition and which are assumed to remain constant with strain. The former contribution is considered to be due to the stored dislocation density. Assuming k=1, which may be reasonable for a high volume fraction of weak obstacles (interstitial and solute atoms) together with a low density of strong obstacles (dislocations) (Kocks, 1980), Eq. (3) can be rewritten as

$$\sigma = \sigma_a + A_I \hat{\sigma}_I + A_\ell \hat{\sigma}_\ell \qquad (7)$$

with the s-values defined in Eq. (5).

Figure 4 shows yield stress measurements in Nitronic 40 stainless steel samples prestrained at 295K to ϵ=0.10 at $\dot{\epsilon}=10^{-3}$ s^{-1} and at $\dot{\epsilon}=5000$ s^{-1}. The results are similar to those reported in copper in that the data for the two prestrain strain rates fall along distinct curves, showing a strain-rate dependence to strain hardening as described by Eq. (6). Analysis of yield stress data for material in the well annealed condition (where the dislocation density is assumed to equal zero) gives σ_I=1204 MPa, p_I=0.667, q_I=1.0, $\dot{\epsilon}_{0I}$=0.155, and $\dot{\epsilon}_0$=10^9 s^{-1}. The curves in Fig. 4 are derived from Eqs. (5) and (7), assuming, p_ℓ=0.667, q_ℓ=1.0, and $\dot{\epsilon}_{0\ell}$=1.0, and give σ_ℓ=283 MPa for the quasi static prestrain and σ_ℓ=360 MPa for the dynamic prestrain.

One difference between the copper results and the results in Nitronic 40, however, is that at high strain rates the strain rate dependence of strain hardening appears to level off in Nitronic 40 rather than increase as noted in copper and nickel (see Fig. 3). We suspect that the tendency for this material to deform by twinning at the higher strain rates is related to this difference, but this needs to be verified. The contribution of deformation twinning will be discussed in more detail in the next section.

4 APPLICATION TO BCC METALS

Dislocation motion in a bcc lattice is opposed by a large Peierls barrier which leads to the strongly rate dependent yield stress observed in metals with this crystal structure. The generation and storage of dislocations

through strain hardening then gives a second contribution to the flow stress in pure bcc metals. Thus, even pure bcc metals are complicated by k=2 in Eq. (3). Fortunately, the combination of many weak obstacles (Peierls barrier) with a few strong obstacles (dislocations) is well represented by n=1 in Eq. (3) such that Eq. (7) again applies. Thus, the analysis procedure in pure bcc metals is identical to that described for Nitronic 40. Figure 5 shows reload yield stress measurements in annealed and quasi-statically and dynamically deformed magnetic iron. The solid lines are fits to Eqs. (7 and 5). We assume that in the annealed condition the dislocation density is negligible so that for these data σ_ε=0. Choosing p=x, q=y, and $\dot{\varepsilon}_o$=10^7 s^{-1} (which for simplicity will be assumed to apply to both contributions), a least squares fit gives σ_I=xyz and g_o=xyz. Treating these as constant, the data for the deformed samples can be analyzed to establish σ_ε. We choose $g_{o\varepsilon}$=1 as representative of the higher activation energy characteristic of dislocation/dislocation interactions. The solid line through the data for the prestrained samples in Fig. 5 gives the fit to the data according to this procedure with σ_ε=xyz.

The interesting result in pure iron, which is independent of the analysis described above, is that there is no clear strain-rate dependence to the hardening observed in Fig. 5. This is in contrast to the results reported in the fcc metals (see Fig. 4). Figure 6 shows similar data in 4340 steel in the normalized and slow cooled (partially spherodized - not martensitic) condition. The data in this figure are complicated by the difference in the measurd prestrain strains, but the results tend to suggest that in 4340 steel, the strain-rate dependent hardening has reappeared.

Figures 7 and 8 show photomicrographs taken from typical areas on quasi-statically and dynamically deformed iron samples, respectively. The difference in twin density in these two micrographs is striking. Twinning is a deformation mechanism that is found in many materials, particularly low stacking fault energy fcc metals (such as the austenitic stainless steels) and in bcc metals where the high temperature and strain-rate sensitivity of the yield stress can lead to high stresses (exceeding the stress required to nucleate and grow twins) at low temperatures and high strain rates. The accomodation of strain by twinning would lead to a lower stored dislocation density and thus a lower hardening rate as expressed by Eq. (6). Conversely, if twin boundaries provide an obstacle to dislocation glide, then the yield stress could increase. In pure iron, the former likely dominates, and as a result the high hardening (dislocation storage) rate found at low strains in fcc metals disappears. Whereas pure iron deforms easily by twinning at high strain rates, the fine, partially spherodized microstructure in the 4340 steel inhibits twin formation. Indeed, metallographic examination of quasi-statically and dynamically deformed 4340 steel specimens showed no evidence of twin formation. It is interesting that in these samples the strain rate dependent initial hardening rate is again observed.

Deformation twinning is also found to strongly affect the deformation of isotropic alpha uranium. The influence of twinning on the application of the mechanical threshold stress model in this metal is described in another contribution in this Conference Proceedings (Armstrong et al, 1989).

Measurement of the mechanical threshold stress at low strains in samples deformed at widely different strain rates gives an indication of the magnitude of the strain rate (and, perhaps, temperature) dependent

hardening. Measurements over a wide strain range are required, however, to fully evaluate the suitability of Eq. (6) in describing strain hardening. This work is currently underway in pure iron and 4340 steel.

5. SUMMARY

A constitutive formalism for deformation over a wide range of strain rates, temperatures, and strains has been applied to several pure fcc metals and to several fcc alloys. The formalism is based on the use of internal state variables and a phenomenological understanding of the kinetics of dislocation glide, dislocation storage, and dynamic recovery. Experimental techniques have been established to measure the internal state variables and the activation energies that characterize dislocation/obstacle interactions. These techniques involve measurement of the temperature and strain-rate dependent yield stress in samples deformed according to various strain rate, strain, and temperature histories. Because we are mostly interested in the behavior at high strain rates, we restrict our yield stress measurements to room temperature and below. Yield stress measurements in the Hopkinson bar are inaccurate and are not included in the correlations, except in materials with very low strain hardening rates which allow accurate back-extrapolated definitions of yield stress.

An underlying concept of the analysis is that we wish to establish correlations that are valid in a certain mechanistic regime, and we restrict the analysis to this regime. For example, the formalism as outlined in section 2 is not capable of describing high temperature, low strain rate (creep) deformation. The contribution of dynamic strain aging also can complicate the analysis. However, the elevated temperature, high strain rate behavior may be well described by correlations established by low temperature, low to medium strain rate experiments because of the strong strain-rate dependencies of diffusion-controlled processes.

The use of metallography and transmission electron microscopy is another means to check that the deformation mechanisms that are modeled are indeed active. This was illustrated by the clear differences in the microstructures in deformed iron shown in Figs. 7 and 8.

The rapid dislocation generation rates observed at high strain rates in copper and nickel may be a general phenomenon in fcc metals, although the contribution of deformation twinning can offset this effect. Work in bcc metals is just beginning. Similar trends to those found in fcc metals are observed in iron and 4340 steel. The description of deformation twinning, particularly the associated kinetics, the influence on strain hardening, and the balance between deformation by twinning versus that by glide, represents a challenge for a complete deformation theory for the high strain rate regime.

ACKNOWLEDGEMENT

This work was supported by the United States Department of Energy, Office of Basic Energy Sciences, Division of Materials Sciences and was performed under the auspices of the United States Department of Energy. The author is grateful to M. Lopez and W. Wright for technical support on the work described herein.

REFERENCES

Armstrong, P E, Follansbee P S, Zocco T 1989 4th Conf Mech Prop High Rates of Strain, this volume

Follansbee P S, Regazzoni G, Kocks U F 1984 Inst Phys Conf Ser No 70 3rd Conf Mech Prop High Rates of Strain (Inst Phys, London) 71

Follansbee P S 1986 Metal Appl of Shock-Wave and High-Strain-Rate Phenom, Murr, Staudhammer, Meyers, eds (Marcel Dekker, NY) 451

Follansbee P S, Kocks U F, Regazzoni G 1985 Mech and Phys Behav of Mater under Dyn Loading, Jour de Phys 46 C5-25

Follansbee P S 1988a Imp Loading and Dynamic Behaviour of Mater, Chiem, Kunze, Meyer, eds. (Verlag) 315

Follansbee P S 1988b Shock Waves in Cond Matter 1987 Schmidt, Holmes eds (Elsevier Publ, NY) 249

Follansbee P S, Kocks U F 1988 Acta Metall 36 81

Follansbee P S, Gray G T III 1989 Metal Trans in press

Follansbee P S, Huang J Gray G T III Acta Metall submitted

Kocks U F 1976 ASME Jour Engng Mater Technol 98 76

Kocks U F 1980 Strength of Metals and Alloys Haasen, Gerold, Kostorz, eds (Pergamon Press, Toronto) 1661

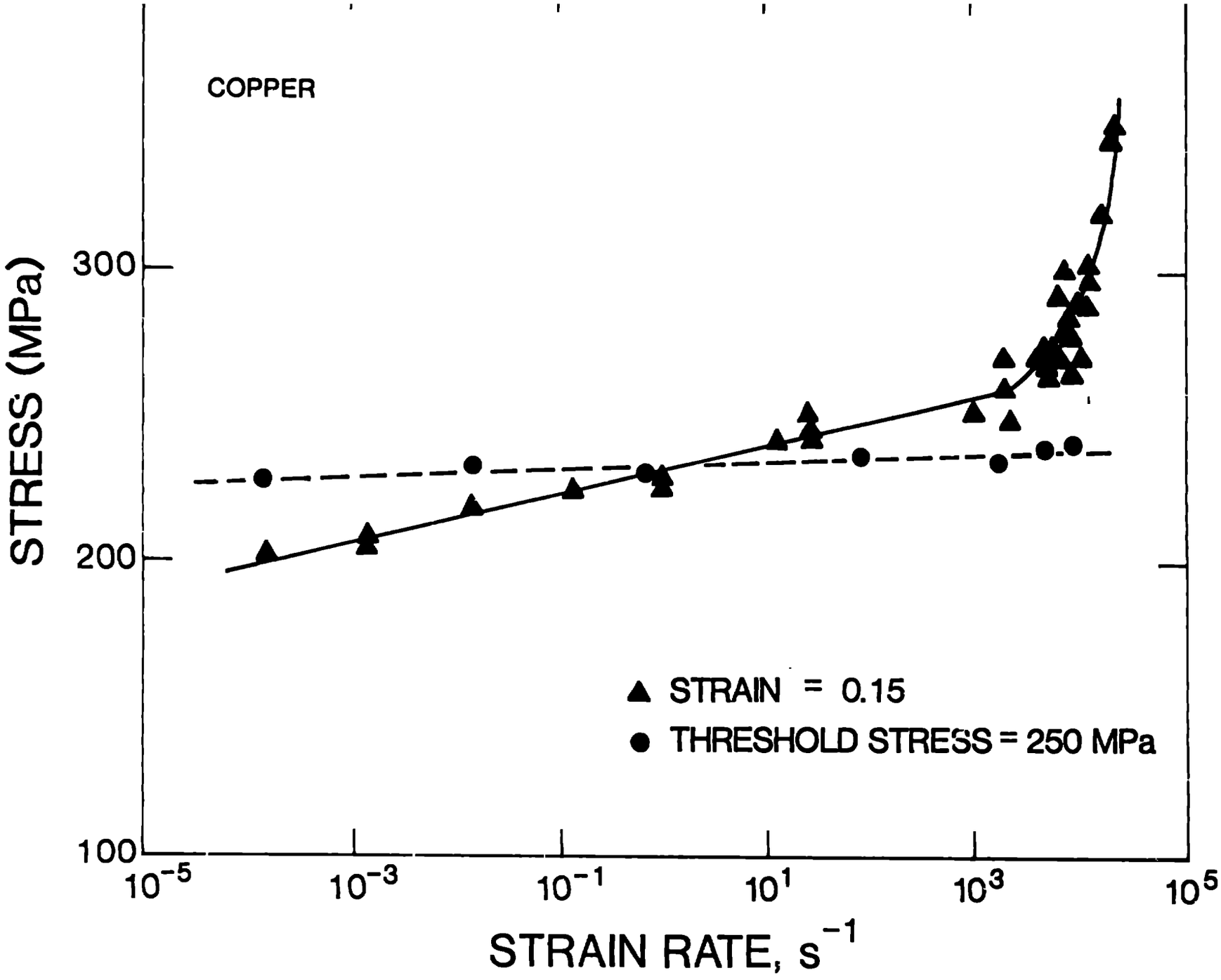
COPPER
STRESS (MPa)
300
200
100
▲ STRAIN = 0.15
● THRESHOLD STRESS = 250 MPa
10^{-5}
10^{-3}
10^{-1}
10^{1}
10^{3}
10^{5}
STRAIN RATE, s^{-1}

Fig. 2

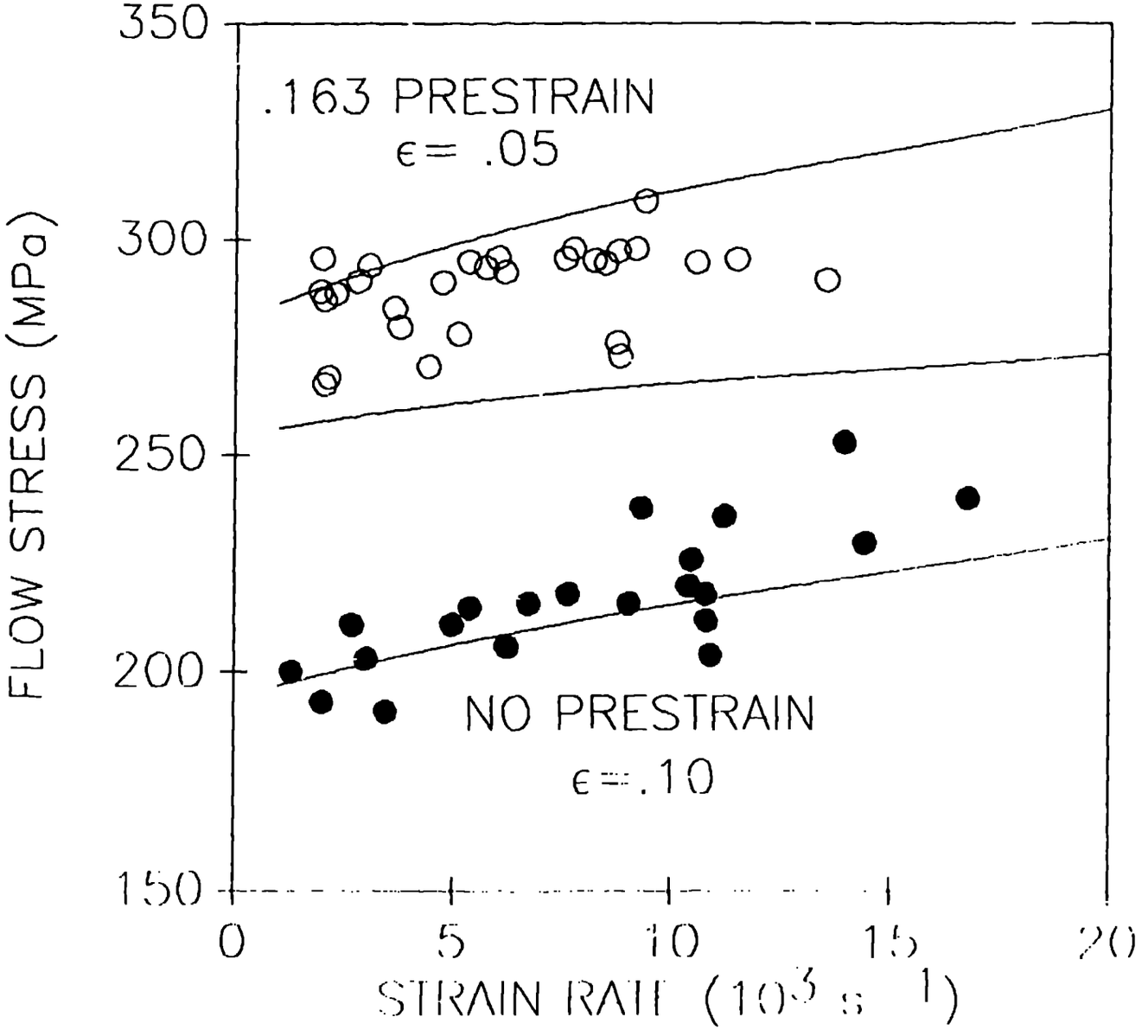
350
300
250
200
150
.163 PRESTRAIN
ϵ= .05
NO PRESTRAIN
ϵ=.10
FLOW STRESS (MPa)
0
5
10
15
20
STRAIN RATE (10^3 s^-1)

Fig. 3

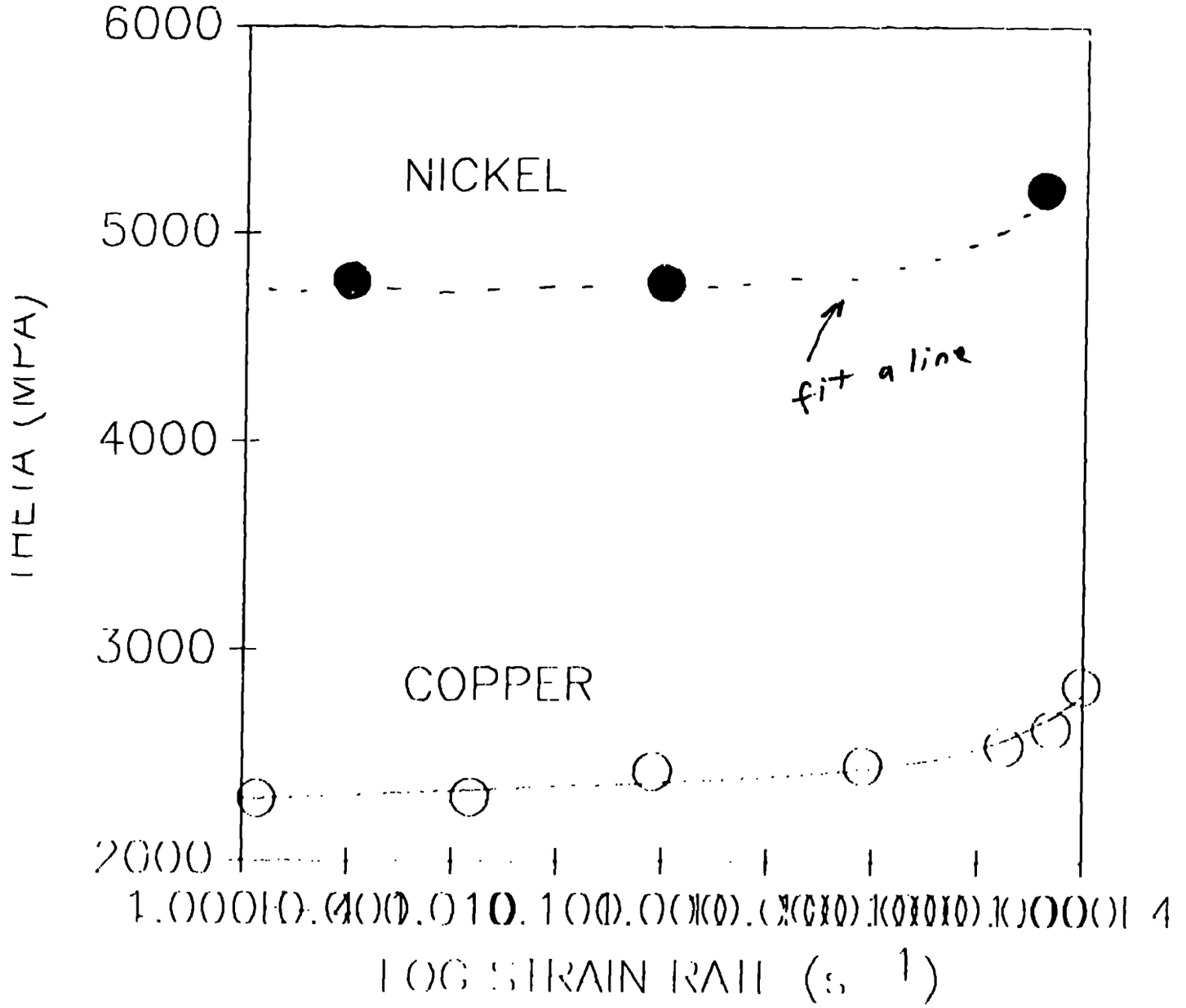
6000
5000
4000
3000
2000
NICKEL
COPPER
fit a line
THETA (MPA)
LOG STRAIN RATE (s⁻¹)

fig. 4

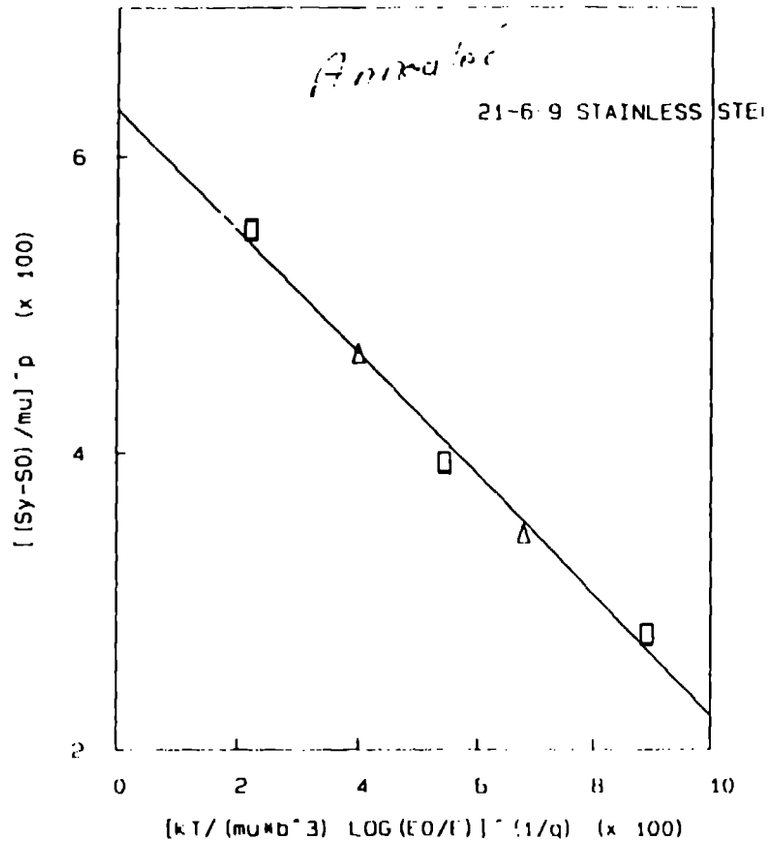

Combine all three into one plot.

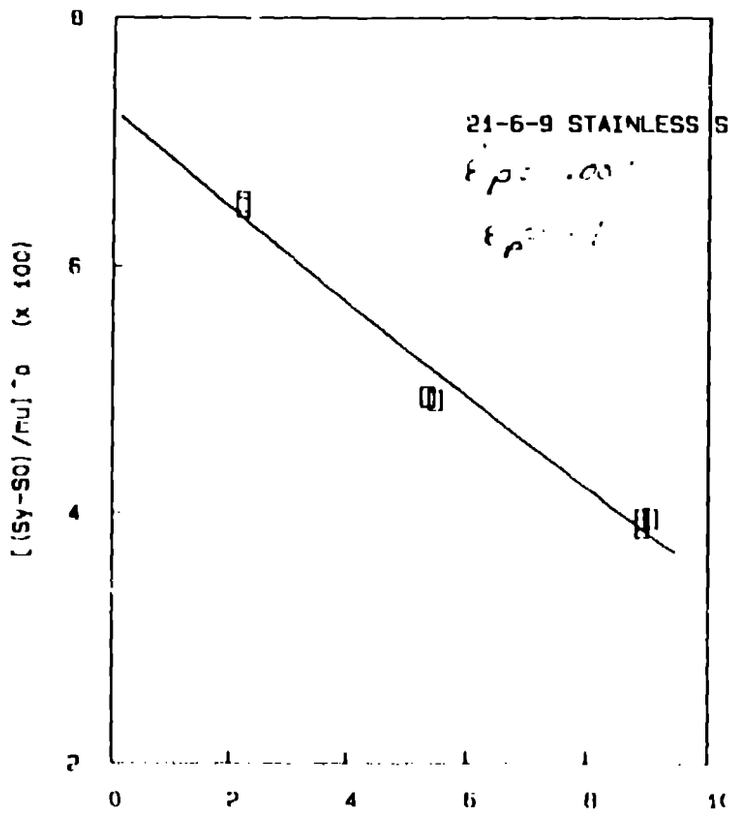

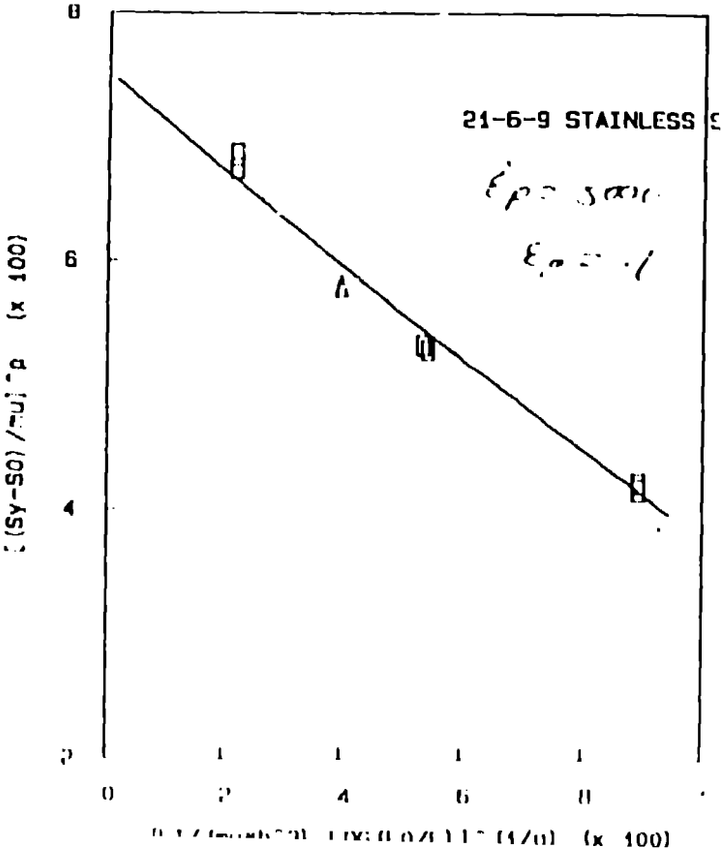

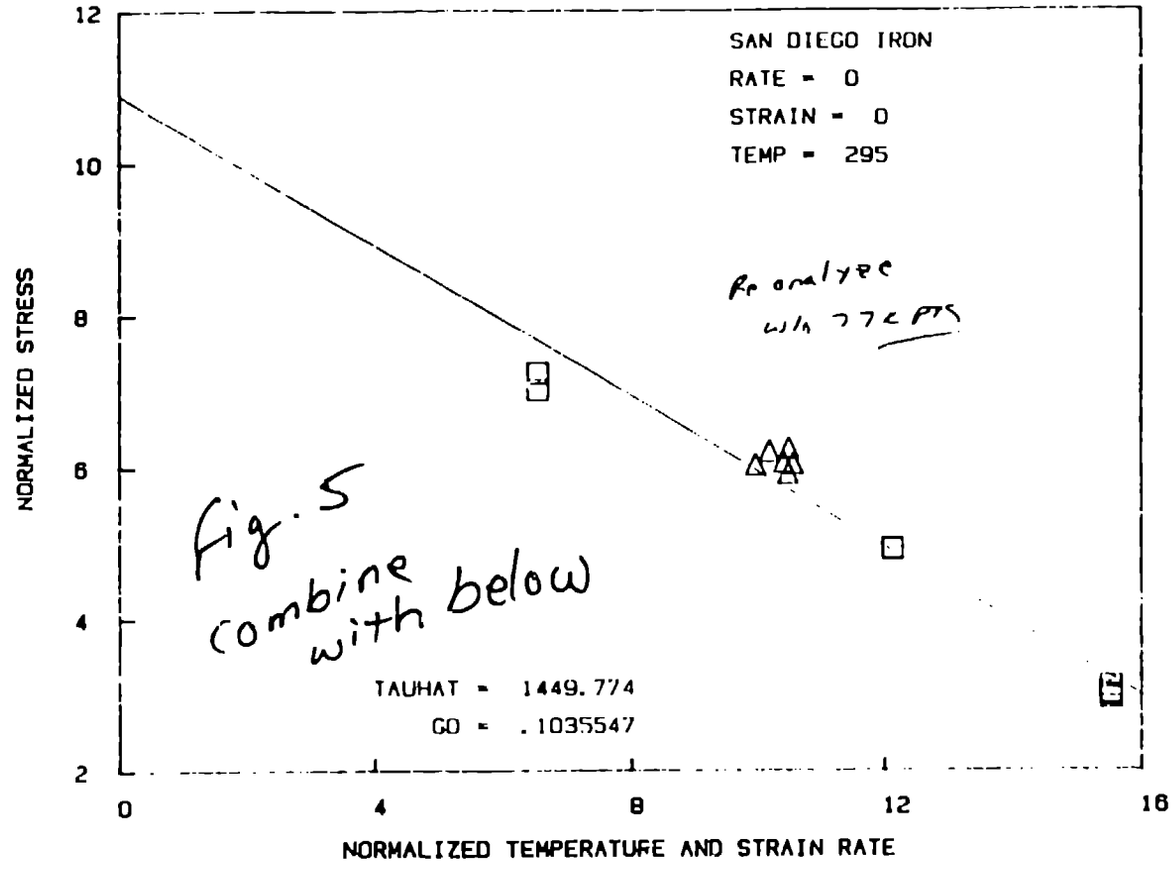

Re analyze w/ 7 pts

fig. 5 combine with below

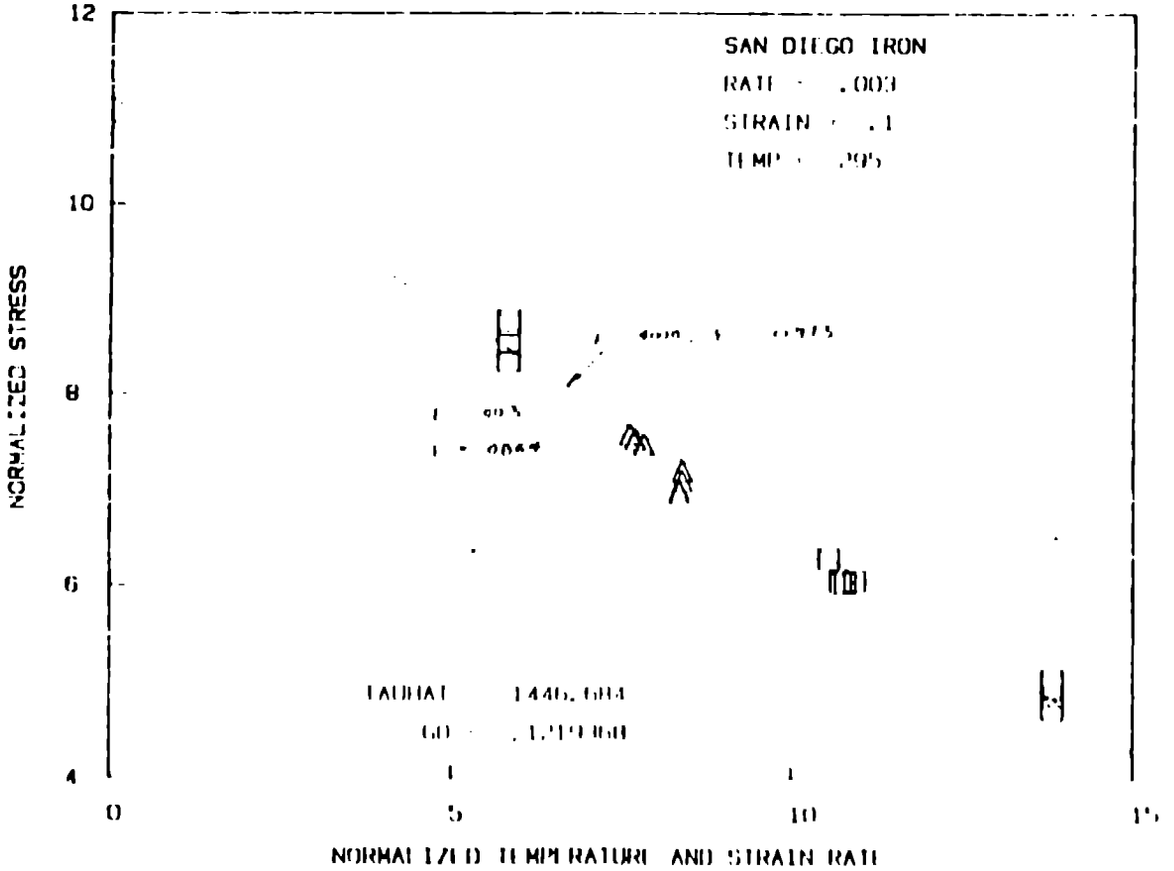

Fig. 6

Redo Add 4340 steel data

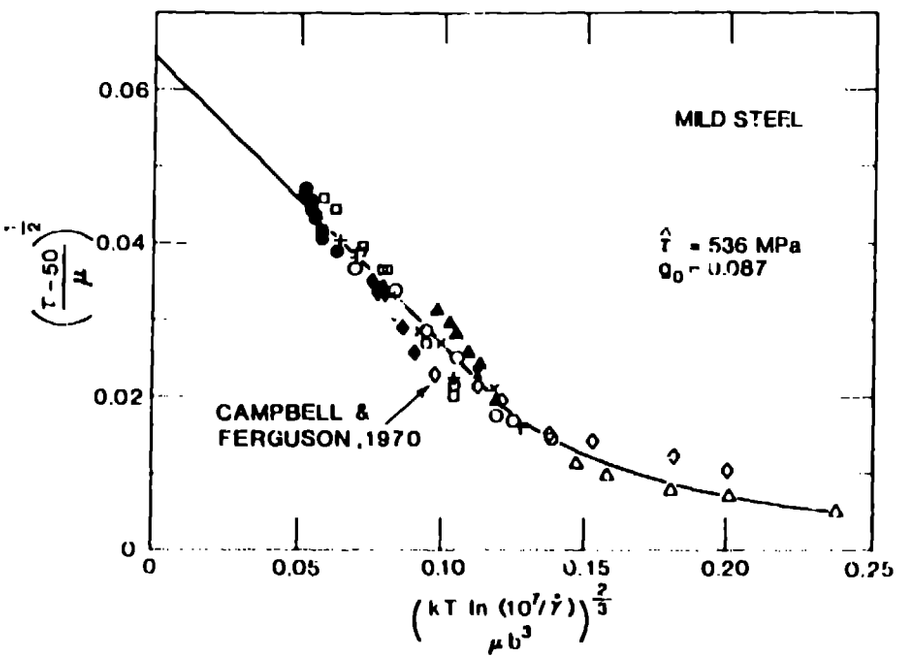

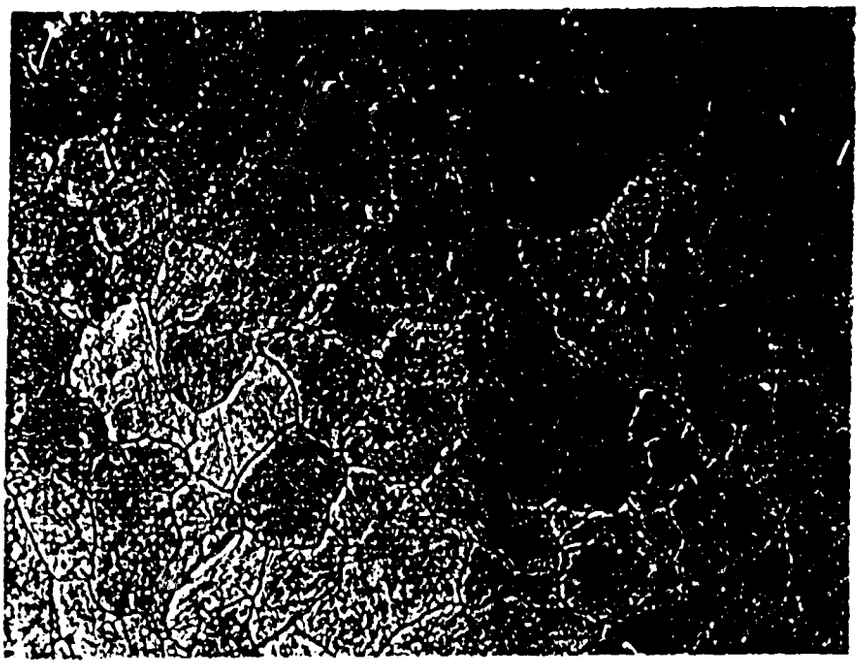

Fig 7

$\dot{\varepsilon} = .001\ s^{-1}$

Fig 8

$\dot{\varepsilon} = .001\ s^{-1}$

twins!